

Enhanced XFEM for crack deflection in multi-material joints

N. Stein · S. Dölling · K. Chalkiadaki ·
W. Becker · P. Weißgraeber

Received: 6 March 2017 / Accepted: 29 June 2017 / Published online: 10 July 2017
© Springer Science+Business Media B.V. 2017

Abstract In this work, an enhanced eXtended finite element method (XFEM) implementation is outlined. It allows for modeling two-dimensional crack growth including potential crack deflection at significantly tougher constituents of multi-material continua. At such material interfaces a user-defined crack deflection criterion is utilized that allows for crack deflection parallel to the interface but is also able to model crack growth that again diverges from the interface. The enhanced XFEM implementation is illustrated analyzing crack growth in a plate with two interacting inclusions showing a distinct toughening effect. Moreover, several different adhesive joint design studies are used to validate the model. The results show that the present XFEM implementation allows for an accurate strength and realistic crack pattern prediction in joint designs of complex shape, e.g. with fillets or rounded adherend corners. The given framework is general and could also be applied to the study of fracture processes including crack deflection as e.g. micro-mechanical fracture

in fibre-reinforced composites or cracks around inclusions.

Keywords Adhesive joints · Crack patterns · Crack deflection · Joint strength · Extended finite element method

1 Introduction

There has been a great demand for predictive modeling approaches addressing the failure loads and corresponding crack patterns in complex adhesive joint configurations. Many works in literature investigated methods to improve the joint strength using complex joint end geometries and adherend shapes. Including a fillet at the joint end, for instance, spreads the load transfer over a larger area and provides a more uniform load transfer as schematically depicted in Fig. 1. Adams and Peppiatt (1974) studied axially loaded single lap joints with a 45° triangular fillet and found that the maximum principal stress was reduced by 40% compared to joints with square ends. Adams and Harris (1987) experimentally investigated aluminum/epoxy single lap joints and found that including a fillet increased the failure load by over 50%. Crocombe and Adams (1981) as well as Tsai and Morton (1995) have shown that the peel and shear stress concentrations are significantly reduced at the overlap end due to an adhesive fillet. Introducing a fillet, however, only reduces the stress concentrations, but does not make them disappear. In adhesive joints

N. Stein (✉) · S. Dölling · W. Becker
Fachgebiet Strukturmechanik, Technische Universität
Darmstadt, Franziska-Braun-Straße 7, 64287 Darmstadt,
Germany
e-mail: stein@fsm.tu-darmstadt.de

K. Chalkiadaki
Automotive Electronics, Robert Bosch GmbH,
Schwieberdingen, Germany

P. Weißgraeber
Corporate Research and Advance Engineering, Robert Bosch
GmbH, Renningen, Germany

with fillets, crack onset is prone to occur at the adherend sharp corners within the adhesive layer at which a stress concentration is present (da Silva et al. 2011). The occurrence of strong stress concentrations can be prevented by rounding the adherend corners as depicted in Fig. 2. The impact of rounded adherend corners has been studied by Adams and Harris (1987) as well as Zhao et al. (2011a, b). They found that adhesive joints with large radius adherend corners show an up to 40% increase in joint strength compared to joints with square ends. Moreover, different crack patterns depending on the adherend corner curvature radius appeared in their experimental studies. For small curvature radius, the crack still initiated at the adherend corner within the adhesive, showing a similar crack pattern as the joints with square ends. For large curvature radius, the locus of failure was either shifted to the outer surface of the fillet or to the curved surface of the rounded adherend corner. Another powerful technique to increase the joint strength is the inclusion of different adherend shapes such as outside or inside tapers that reduce the local stiffness of the joint. Adams et al. (1986) as well as da Silva and Adams (2007) studied, for instance, various double lap joint configurations and found that incorporating an internal taper and adhesive fillet can triplicate the failure load. Similar work has been done by Hildebrand (1994) on single lap joints with fibre-reinforced plastics and metal adherends. The results indicated, that a significant increase of the joint strength can be obtained by using a careful joint end design. A comprehensive overview on expedient techniques can be found in the textbook on adhesion technology by da Silva et al. (2011). Though many works address the strength prediction of complex joint geometries, no general model accurately predicting the corresponding crack patterns has been established so far. Yet, the knowledge of the arising crack pattern is especially important for an insight of the underlying failure process required for an adequate joint design.

Most of the current failure models for adhesively bonded joints are either based on strength of materials approaches, fracture mechanics approaches or damage mechanics. Strength of materials approaches evaluate allowable equivalent stress (Harris and Adams 1984; Bigwood and Crocombe 1990) or strain quantities (Goglio et al. 2008; da Silva et al. 2009) using analytical models or the finite element method (FEM). Comparing the stress or strain quantities to a critical material strength yields the corresponding joint

strength. However, these approaches cannot directly be applied to structures featuring strong stress concentrations as they arise at the bi-material notches in adhesive joints. Fracture mechanics approaches using linear elastic fracture mechanics (LEFM) are capable of dealing with singularities but require an initial pre-existing crack for calculating the strain energy release rate or stress intensity factors (Fernlund and Spelt 1991; Shahin and Taheri 2008). Hence, the results strongly depend on the size of the assumed initial crack size.

In recent years, cohesive zone models (CZMs) have been successfully used for analyzing failure in adhesive joints (Liljedahl et al. 2006; Turon et al. 2007; Campilho et al. 2011b, 2013a) since they allow for simulating damage onset and growth along pre-defined crack paths in arbitrary joint configurations. The shortcomings of strength of materials and fracture mechanics approaches are circumvented by CZMs. That is, CZMs can be applied to engineering structures exhibiting strong and potentially singular stress concentrations without the requirement of a pre-existing crack. Damage initiation and propagation are described by a local non-linear traction-separation law that controls the local degradation of the stiffness. In its simplest form, it is determined by two fracture parameters: the material strength that must be exceeded for damage initiation, and the fracture toughness that controls the damage propagation. In this way, CZMs consider a stress criterion in combination with an energy criterion. However, it is to note that the crack path has to be known a priori. For an accurate failure prediction, a regularization parameter has to be determined to control convergence issues (Turon et al. 2007; da Silva and Campilho 2012). A detailed introduction to CZMs and their applications to adhesive joints can, for instance, be found in the textbook by da Silva and Campilho (2012).

Another approach combining stress and energy criteria without the need of a pre-existing crack is given by the coupled stress and energy criterion proposed by Leguillon (2002) in the framework of Finite Fracture Mechanics (FFM). However, the underlying physical failure process is a different one compared to damage mechanics approaches: an instantaneous formation of a finite sized crack is assumed. Although the approach has been successfully applied to adhesive joints (Moradi et al. 2013; Hell et al. 2014; Stein et al. 2015, 2016), it is restricted to brittle adhesives. Moreover, a full numerical implementation requires a huge computa-

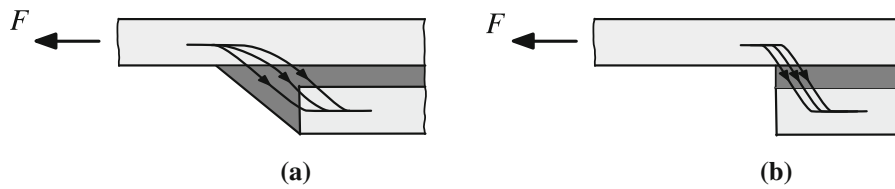


Fig. 1 Enlarged section of axially loaded single lap joints with fillet **(a)** and without fillet **(b)** schematically showing the concentrated load transfer at the overlap end. **a** Joint with fillet. **b** Joint with square ends

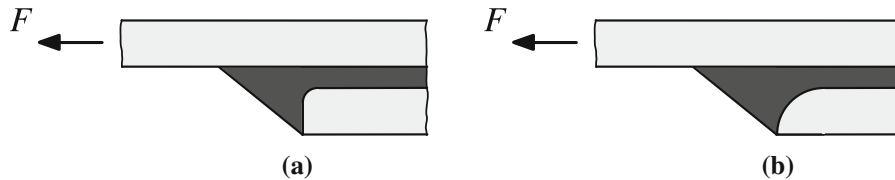


Fig. 2 Enlarged section of axially loaded single lap joints with fillets and rounded adherend corners with **a** small curvature radius and **b** large curvature radius

tional effort. A detailed overview on applications of the coupled criterion can be found in the review article by [Weigraaber et al. \(2016\)](#). More recently, the eXtended finite element method (XFEM) has been employed for modeling damage growth in adhesive joints. Incorporating a CZM in the XFEM framework, neither a pre-existing crack nor a pre-defined crack path has to be defined. Cracks are allowed to grow independently within a bulk region of a material without the requirement of expensive remeshing. The XFEM, first proposed by [Belytschko and Black \(1999\)](#) as well as [Mos et al. \(1999\)](#), extends the conventional FEM introducing additional local enrichment functions in the vicinity of the crack to account for the displacement jump and near-tip field of the crack. In the conventional FE software package Abaqus, a cohesive segments approach ([Remmers et al. 2008](#)) within the framework of XFEM based on a traction-separation cohesive behaviour is implemented for modeling crack initiation and propagation. This approach combines the idea of CZM with XFEM introducing cohesive segments perpendicular to the maximum principal stress in elements in which a damage initiation criterion is satisfied. In recent works, this approach has been used by [Campilho et al. \(2011a, b, 2013b\)](#) as well as [Fernandes et al. \(2015\)](#) in order to predict crack patterns and corresponding failure loads of adhesive joints. They found that the approach yields physically reasonable crack patterns only for DCB specimens but not for adhesive single and double lap joints. In the XFEM analysis of the

latter, the crack initiated within the adhesive close to the adherend where a stress singularity is present but subsequently propagated into the adherend. Moreover, they were able to determine failure loads for single lap joints only by restraining the crack direction or proposing that the crack initiation load corresponds to the failure load. [Stuparu et al. \(2016a, b\)](#) as well as [Mubashar et al. \(2014\)](#) went one step forward and introduced CZMs at the adherend-adhesive interface in addition to the XFEM enrichment. This way, they were able to predict crack patterns in axially loaded single lap joints with fillets. However, in the works by [Stuparu et al. \(2016a, b\)](#) an initial delamination for modeling crack propagation is introduced and in the studies by [Mubashar et al. \(2014\)](#) the modeling approach is validated against only one experiment. If the crack once meets the interface in the proposed XFEM frameworks, it is not possible that it will leave it again. Furthermore, it is unclear how a crack should be treated if the XFEM crack meets the center of a conventional cohesive element in the Abaqus framework.

The present work provides an enhanced XFEM framework that allows for a prediction of the failure load and corresponding crack pattern and surpasses the limitations of the above mentioned approaches. Using the User Subroutine UDMGINI, a crack direction criterion is embedded in the Abaqus XFEM framework that accounts for the crack deflection at bi-material interfaces in adhesive joints. This way, the proposed approach allows for the analysis of arbitrary joint con-

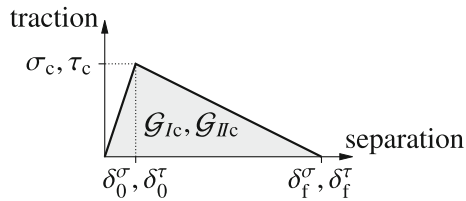


Fig. 3 Bilinear traction-separation law for pure modes. The indices 0 and f denote displacements associated to damage initiation and complete failure, respectively

figurations giving physically reasonable crack patterns and accurate failure load predictions without introducing additional CZMs.

2 Theoretical background

In the following, a CZM approach used for validation in case of single lap joints with square ends and the current XFEM implementation in Abaqus are introduced. For single lap joints with square ends, cracks typically emanate from the reentrant corner and propagate along the interface so that the crack path is known a priori. For more complex geometries as, for instance, joints with fillets or rounded adherend corners, more sophisticated crack patterns are expected. The current XFEM implementation in Abaqus also shows some drawbacks in modeling failure in adhesive joints that are thoroughly discussed in the present work. Nevertheless, the implementation serves as basis for the present enhanced XFEM approach.

2.1 Cohesive zone modeling

A local approach is implemented for the CZM analyses. That is, cohesive elements are used to model interfaces instead of a strip of finite thickness (da Silva and Campilho 2012). Zero-thickness cohesive elements (COH2D4 from Abaqus library) are placed along the interfaces between adherends and adhesive where crack initiation and propagation is expected in single lap joints with square ends. The elements are based on a bilinear traction-separation law as depicted in Fig. 3.

It describes the elastic response up to a peak stress and subsequent linear degradation of the material stiffness until final debonding occurs. The initial elastic stiffness before the subsequent softening is set to 10^7

N/mm³ as proposed by Gonçalves et al. (2000) to avoid any change in the global stiffness. Since failure in single lap joints occurs under mixed-mode loading a quadratic stress criterion as damage initiation criterion is considered

$$\left(\frac{\langle\sigma\rangle}{\sigma_c}\right)^2 + \left(\frac{\tau}{\tau_c}\right)^2 = 1, \quad (1)$$

where σ_c and τ_c are the respective tensile and shear strength and $\langle\cdot\rangle$ are the Macaulay brackets guaranteeing that compressive stresses do not cause damage initiation. If the damage initiation criterion (1) is satisfied a linear softening process starts. Complete separation is finally predicted, if a linear interaction law of the required energy release rates for failure is satisfied

$$\frac{\mathcal{G}_I}{\mathcal{G}_{Ic}} + \frac{\mathcal{G}_{II}}{\mathcal{G}_{IIc}} = 1, \quad (2)$$

where \mathcal{G}_I and \mathcal{G}_{II} are the energy release rates corresponding to the tractions σ and τ , and \mathcal{G}_{Ic} , \mathcal{G}_{IIc} are the respective fracture toughnesses. It is to note that for pure mode loading, the released energy in each mode at complete debonding corresponds to the area under the triangle of the traction-separation law, as shown in Fig. 3. Since convergence issues occur for CZM analyses in Abaqus due to the local stiffness reduction, a regularization parameter for the viscous regularization feature is chosen so that converged results are obtained for each joint configuration. This is achieved by performing a parametric study concerning the failure load with decreasing levels of viscous damping to determine an appropriate viscosity parameter μ . This is especially important for CZM analyses since the incorporated viscosity artificially increases the toughness and typically leads to an overestimation of the failure load if the viscosity parameter μ is not chosen properly. For most configurations, a value of $\mu = 10^{-5}$ has proven to be a good trade-off regarding accuracy and computation time. Moreover, it is important to choose a sufficiently small characteristic cohesive element length l_e to obtain converged failure load predictions (da Silva and Campilho 2012). If the cohesive zone ahead of the crack tip is discretized by too few elements, the stress field in the vicinity of the crack tip is not captured correctly. In order to calculate accurate failure loads a minimum number of cohesive elements is required in the cohesive zone. Since the area of the cohesive zone

is significantly influenced by the adhesive thickness a particular ratio of cohesive element length l_e to adhesive thickness t is recommended. For the investigated configurations, a ratio of $l_e/t = 0.075$ representing an upper bound for the cohesive element length with respect to the adhesive thickness has proven to be sufficient.

2.2 Abaqus implementation of the XFEM

Compared to the conventional FEM, the XFEM provides several advantages regarding the numerical modeling of crack propagation. Using the traditional FEM, propagating cracks are usually modeled implementing extensive remeshing algorithms since the crack geometry has to be aligned with the element edges. In contrast, the XFEM is based on enrichment functions embedded in the finite element formulation that allow for an efficient modeling of the displacement jump between crack faces and corresponding near-tip fields without remeshing. Simultaneously, the approach retains the classical FEM properties such as partition of unity (Melenk and Babuška 1996) and sparsity of the stiffness matrix.

In the framework of the XFEM, the displacement vector \mathbf{u} , including the displacement enrichments, can be given as

$$\mathbf{u} = \underbrace{\sum_{i \in \mathcal{A}} N_i(\mathbf{x}) \mathbf{u}_i + \sum_{i \in \mathcal{B}} N_i(\mathbf{x}) H(\mathbf{x}) \mathbf{a}_i}_{\text{Heaviside enrichment}} + \underbrace{\sum_{i \in \mathcal{C}} \left[N_i(\mathbf{x}) \sum_{j=1}^4 F_j(\mathbf{x}) \mathbf{b}_i^j \right]}_{\text{local crack tip enrichment}} \tag{3}$$

where \mathcal{A} is a set containing all nodes in the mesh, $N_i(\mathbf{x})$ are the nodal shape functions and \mathbf{u}_i is the conventional FEM degree of freedom of node i . \mathcal{B} and \mathcal{C} are subsets of \mathcal{A} containing only the nodes enriched with the generalized Heaviside function $H(\mathbf{x})$ and crack tip functions $F_j(\mathbf{x})$, respectively. The subset \mathcal{B} comprises nodes related to elements that are completely cut by the crack. The generalized Heaviside function $H(\mathbf{x})$ is a function of constant unit magnitude changing its sign across the crack faces physically introducing the discontinuity across the crack. The subset \mathcal{C} contains only nodes related to elements containing the crack tip. The respective crack tip functions $F_j(\mathbf{x})$ are cho-

sen dependent on the particular physics of the crack tip model. The approach (3) with properly chosen crack tip functions can, for instance, be employed to represent a crack in an elastic medium (Belytschko and Black 1999) as well as along a bi-material interface (Sukumar et al. 2004) or impinging on a bi-material interface (Sukumar and Prévost 2003). However, the crack tip functions $F_j(\mathbf{x})$ are only used for modeling stationary cracks in Abaqus which is not in the scope of the present work.

In Abaqus, propagating cracks are modeled using the cohesive segments method (Remmers et al. 2008) settled in the framework of the XFEM. In order to allow for simulating crack propagation along an arbitrary solution dependent path, the displacement ansatz of Eq. (3) is used considering only the Heaviside enrichment. In this approach, it is presumed that the crack propagates across entire elements at a time if a damage initiation criterion is fulfilled. Damage initiation is typically governed by a maximum principal stress criterion

$$\frac{\langle \sigma_I \rangle}{\sigma_c} = 1, \tag{4}$$

where σ_I and σ_c are the largest and maximum allowable principal stress, respectively. The crack direction is always set perpendicular to the corresponding maximum principal stress direction. Cohesive segments are introduced in these elements to model the damage evolution so that modeling the crack tip singularity and the use of the associated crack tip functions are avoided. The damage evolution in the cohesive segments is based on an energetic criterion and a softening law, as e.g. introduced in Sect. 2.1 [Eq. (2) and based on the region of the traction-separation law with decreasing stiffness depicted in Fig. 3, respectively].

The displacement discontinuity of the cracked elements associated to the Heaviside enrichment is implemented using phantom nodes as presented by Song et al. (2006) and Remmers et al. (2008). The phantom nodes are initially superposed on the original real nodes. They subdivide elements cut by a crack if the crack propagates. When a crack propagates through an entire element, the cracked element splits into two parts, each formed by real and phantom nodes, respectively. Each phantom node and associated real node are no longer restrained and can separate according to a cohesive law up to complete failure. An exemplary

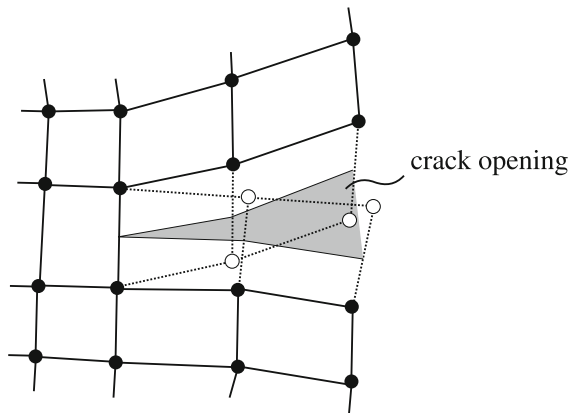


Fig. 4 Representation of a crack opening using phantom nodes following Song et al. (2006). Solid and hollow circles illustrate the original and phantom nodes, respectively

mesh with a crack opening modeled by phantom nodes is depicted in Fig. 4. It is to note, that convergence issues occur if the crack cuts the element in the close vicinity of a node due to the unfavourable size ratio of the newly generated elements. However, an adequate viscous regularization as included for the cohesive elements and discussed in Sect. 2.1 bypasses the numerical problems. If the required regularization imposes a large artificial increase of the predicted failure loads, an alternative mesh should be considered. In most cases, this behaviour is accompanied by a kink in the load-displacement curve and a subsequent increase of the load with respect to the displacement.

As discussed in the works by Campilho et al. (2011b) as well as da Silva and Campilho (2012), this approach leads to severe problems modeling common adhesive joint designs. Regarding, for instance, single and double lap joints under tension, crack onset is correctly predicted at the reentrant corner of adhesive joints with square ends but the crack subsequently tends to propagate into the adherend. The crack direction criterion does not account for the constraining effects imposed by the stiff adherends with comparatively large fracture toughness leading to an unrealistic behaviour of the crack. Especially in the case of metallic adherends, it is obvious that cracks reaching the interface must be deflected along the interface. The works on single lap joints and double lap joints (Campilho et al. 2011b; Fernandes et al. 2015) revealed that the current XFEM implementation in Abaqus is not suitable for simulating damage growth in common adhesive lap

joint configurations. The same conclusion regarding the suitability of the XFEM implementation for adhesive joint analyses was drawn in the study on DCB specimens (Campilho et al. 2011a). Though Campilho et al. (2011a) successfully simulated mode I crack growth using the XFEM approach, they pointed out the limitations regarding mixed-mode fracture.

3 Enhanced XFEM approach for modeling crack deflections

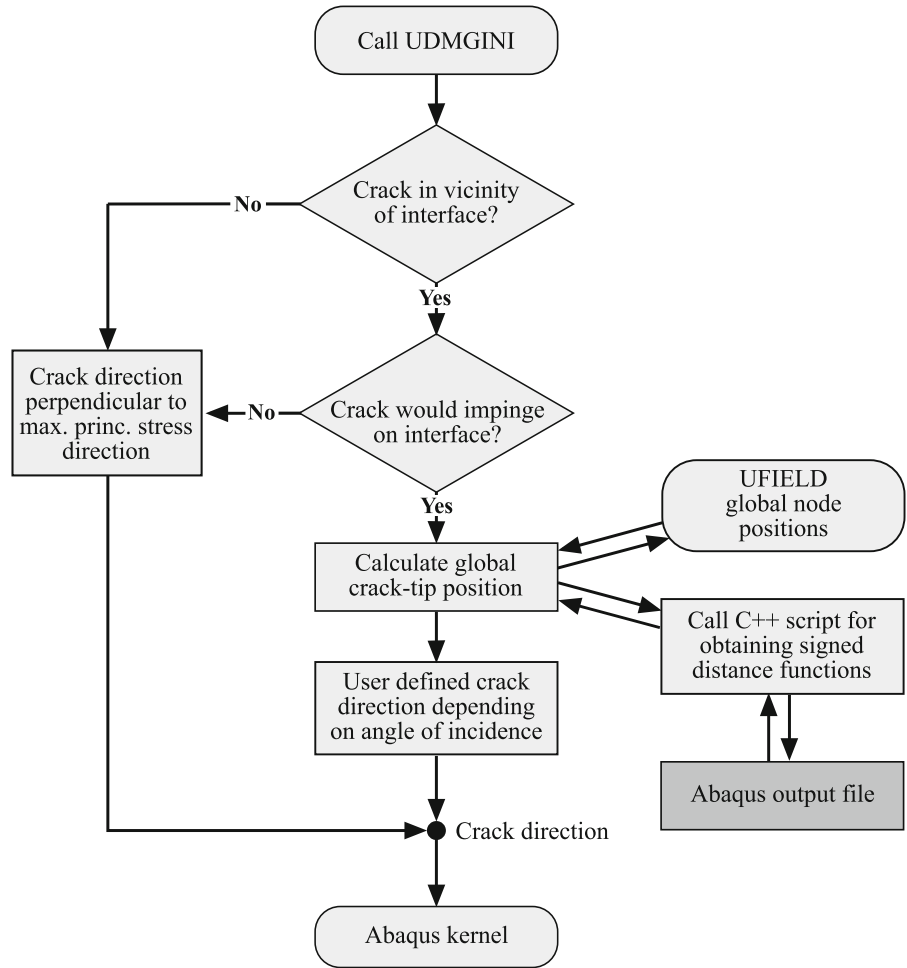
3.1 Modeling approach

In this section, an enhancement of the current XFEM implementation in Abaqus is presented that allows for simulating crack propagation near bi-material interfaces. The limitations of the Abaqus implementation of the XFEM are surpassed. In the following, the procedure and required subroutines directly related to Abaqus are outlined in detail and the required automated pre-processing steps are presented.

Due to the elastic and fracture toughness contrast of adherend and adhesive as typically present in adhesive joints with metallic adherends, it is initially presumed that crack deflection occurs if a crack meets the adherend-adhesive interface. Therefore, only the region associated to the adhesive is modeled using enrichment functions. The main idea of the enhanced XFEM approach consists of detecting the particular situation if a crack would impinge on the bi-material interface and subsequently implementing a user-defined crack direction depending on the angle of incidence. If the crack propagates within the adhesive layer, the conventional choice of the crack direction perpendicular to the maximum principal stress Eq. (4) according to the standard XFEM implementation in Abaqus is used. Hence, only the damage initiation criterion and the choice of the crack direction are altered. The damage evolution follows the same traction-separation law as before, see Sect. 2.2.

Abaqus provides an interface for modeling user-defined damage initiation and crack direction criteria via the subroutine UDMGINI. In order to obtain all required information for calculating a crack direction, the subroutine UFIELD and a C++ script for accessing the Abaqus output file during the computation are additionally necessary in the current implementation. The whole procedure starts with calling UDMGINI for

Fig. 5 Flowchart of the implemented procedure called at each time increment during an Abaqus XFEM analysis



each element of the adhesive layer as depicted in the flowchart in Fig. 5. In elements in which the damage initiation criterion is fulfilled, a cohesive segment is introduced automatically. If the crack is in the close vicinity of the interface and would impinge on the interface using the conventional crack direction, a new user-defined crack direction will be determined. Otherwise, the crack direction perpendicular to the maximum principal stress according to the standard XFEM implementation in Abaqus is used. More specifically, if the crack approaches the vicinity of the interface, a restricted area is introduced into which the crack may not propagate. The restricted area is determined via two auxiliary vectors \mathbf{r}_{lim1} and \mathbf{r}_{lim2} connecting the crack tip position with the center of the edges having one point on the interface as depicted in Fig. 6. Subsequently, it is checked whether the crack direction perpendicular to the maximum principal stress \mathbf{r}_{MPS}

points into the introduced restricted area. Hence, the following expression must be evaluated

$$(\mathbf{r}_{MPS} \times \mathbf{r}_{lim1}) \cdot (\mathbf{r}_{MPS} \times \mathbf{r}_{lim2}) \begin{cases} < 0 & \text{inadmissible crack direction,} \\ > 0 & \text{admissible crack direction.} \end{cases} \quad (5)$$

If the crack direction orthogonal to the maximum principal stress does not point into the restricted area (admissible crack direction), it is used as the new crack direction $\mathbf{r}_{crack} = \mathbf{r}_{MPS}$. Otherwise (inadmissible crack direction), one of the vectors \mathbf{r}_{lim1} and \mathbf{r}_{lim2} are chosen as the new crack direction. In this case, it is distinguished between the two vectors depending on the angle of incidence according to

$$\mathbf{r}_{crack} = \begin{cases} \mathbf{r}_{lim1} & \text{if } \hat{\mathbf{r}}_{MPS} \cdot (\hat{\mathbf{r}}_{lim1} - \hat{\mathbf{r}}_{lim2}) > 0 \\ \mathbf{r}_{lim2} & \text{if } \hat{\mathbf{r}}_{MPS} \cdot (\hat{\mathbf{r}}_{lim1} - \hat{\mathbf{r}}_{lim2}) < 0 \end{cases}, \quad (6)$$

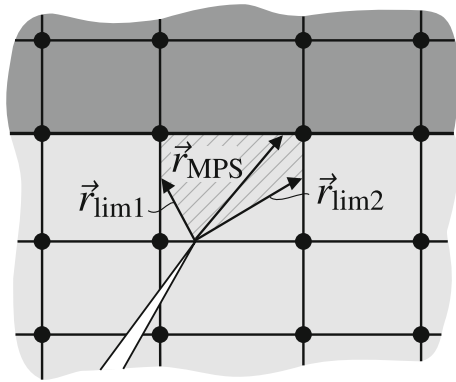


Fig. 6 Schematic illustration of the treatment of a crack approaching the vicinity of a bi-material interface. The *dashed region* represents the restricted area spanned by the vectors $\mathbf{r}_{\text{lim}1}$ and $\mathbf{r}_{\text{lim}2}$

where $\hat{\mathbf{a}} = \mathbf{a}/|\mathbf{a}|$. As a final result, the subroutine delivers the crack direction as an output quantity which is transferred to the Abaqus kernel for the next step. It is worth mentioning, that the vectors spanning the restricted area are defined via the center of the edges having one point on the interface. This way, convergence problems and unfavourable size ratios of newly created elements are avoided as discussed in Sect. 2.2.

In this way, it is possible that a crack propagating along the interface can exit the vicinity of the material transition in contrast to the coupled CZM-XFEM approaches proposed by Mubashar et al. (2014) and Stuparu et al. (2016a,b). For determining the user-defined crack direction, the global crack-tip position is required. Unfortunately, neither the nodal coordinates of the mesh nor the global crack-tip position are directly available in the Abaqus user subroutine interface. Abaqus internally provides a description of the crack geometry using the level set method (Osher and Sethian 1998). The crack geometry is defined by two signed distance functions locally describing the crack surface and crack front. Hence, an efficient C++ script is used to access the output database of Abaqus during the computation and to extract the nodal values of the signed distance functions. In addition, the subroutine UFIELD is employed to obtain the nodal coordinates of the mesh.

In a pre-processing step, the mesh topology is extracted from the input file. A routine arrays the topology and saves it as ASCII file such that the user subroutine can access the required information and efficiently

decide whether a crack is located in the vicinity of an interface and is possibly impinging on an interface.

The combination of the scripted pre-processing and the subroutine is implemented for performing an enhanced XFEM analysis. Only a conventional input file has to be generated and provided as input for the complete framework. Subsequently, the framework automatically performs the pre-processing and runs an analysis including the user subroutine with the procedure described above. As an outcome, the failure load and corresponding crack pattern are obtained.

3.2 Example

In order to illustrate the procedure, crack growth in a plate with two inclusions is investigated as a typical crack interaction example. A composite plate with a pre-crack under tensile loading F , as shown in Fig. 7a, is analyzed. The plate consists of a matrix (Young's modulus $E_1 = 3.5$ GPa, Poisson's ratio $\nu_1 = 0.33$, strength $\sigma_c = 70$ MPa, toughness $\mathcal{G}_c = 0.35$ N/mm) reinforced with two particles ($E_2 = 70$ GPa, $\nu_2 = 0.3$). For this configuration, it is a priori known, that the crack propagates only through the matrix and not through the particles. As input, the framework requires only the input file of the structural configuration with corresponding failure parameters in order to start an enhanced XFEM analysis. Starting from the pre-crack, the crack propagates perpendicular to the maximum principal stress towards the left particle, cf. Fig. 7b. Using the classical XFEM approach implemented in Abaqus, the crack would penetrate the interface and propagate through the particle after several increments with load increase. In the framework of the enhanced XFEM approach, the crack is deflected via the implemented user-defined crack direction in the vicinity of the bi-material interface. Shortly after passing the centerline of the first particle, the crack propagates perpendicular to the maximum principal stress again and leaves the vicinity of the interface. Approaching the second particle, the crack shows a similar behaviour until the plate is completely fractured. Besides providing the calculated crack pattern and corresponding failure load, the enhanced XFEM framework correctly covers physical effects such as the toughening effect of particle reinforcements. Literature (Kitey et al. 2006; Bush 1997; Wang et al. 2012) shows, that a crack approaching a stiff inclusion may experience a so called

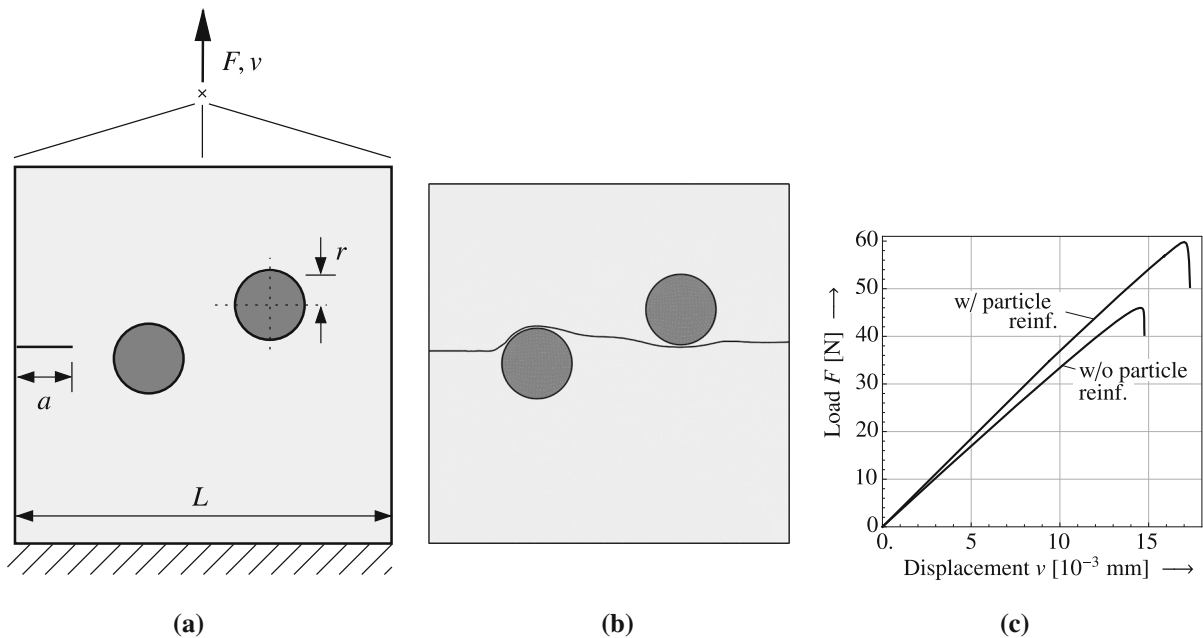


Fig. 7 Analysis of crack growth in a particle reinforced composite plate with the dimensions $L = 1 \text{ mm}$, $a = 0.1L$, $r = 0.2L$: **a** the structural configuration, **b** the corresponding crack pattern

shielding effect. The corresponding energy release rate is reduced compared to the case of a nonreinforced plate. This shielding effect causes an increased effective toughness. Finally a larger stiffness and higher failure load of the reinforced structure are predicted, as shown in Fig. 7c, which is a typical physical phenomenon of particle reinforcement composite materials (Chawla and Shen 2001).

4 Joint design analyses

A numerical analysis using the commercial finite element software Abaqus is performed in order to predict the joint strength and crack patterns in various adhesive single lap joint configurations. In the present work, three types of adhesive single lap joints are studied: single lap joints with square ends, with full depth fillets and with rounded adherend corners in addition to fillets. The characteristic dimensions and boundary conditions are depicted in Fig. 8. The boundary conditions consist of clamping the joint at the upper adherend left end and implementing a vertical restraint and a horizontal tensile load at the lower adherend right end. Geometrically non-linear analyses are carried out to capture the large bending deformations of the

and **c** the load-displacement curve showing a pronounced toughening effect

adherends due to the eccentric load path. Linear elastic material behaviour is considered for adhesive and adherends. Two-dimensional models of the single lap joints using 4-node plane strain solids elements (CPE4 from Abaqus library) for the computational meshes are implemented. The meshes for all models are generated employing the automatic meshing algorithms of Abaqus with smaller sized elements approaching the overlap region to ensure the convergence of the investigated quantities. A representative mesh used in this study is shown in Fig. 9.

In the following, the predicted failure loads and crack patterns for different axially loaded adhesive single lap joint designs are compared to experimental results from literature. Only experimental results in which no adherend yielding or failure initiation in the adherend occurred as well as comparatively brittle adhesives are considered. Incorporating adherend plasticity and an appropriate failure criterion is generally possible in the presented framework but goes beyond the scope of the present work and is not necessarily required for validation of the enhanced XFEM approach. The results for single lap joints with square ends are additionally compared to numerical results calculated with a CZM approach. The particular joint dimensions and

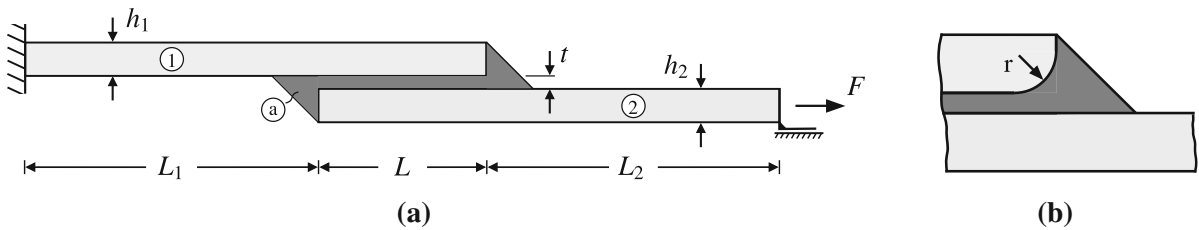
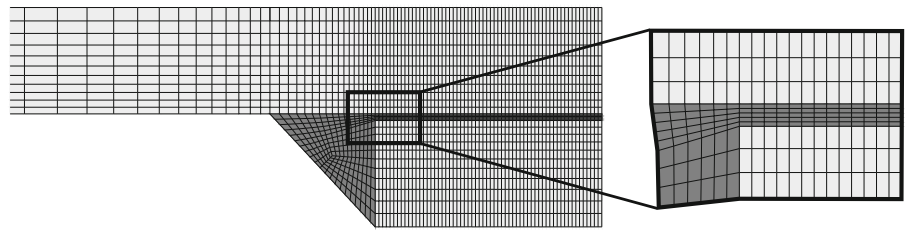


Fig. 8 Dimensions and boundary conditions of the considered adhesive single lap joints under tensile loading F . The geometry is characterized by the respective adherend thicknesses h_1 and h_2 , the adhesive thickness t , the overlap length L , the respective

unsupported adherend lengths L_1 and L_2 , the joint width b and the curvature radius r . **a** Axially loaded single lap joint with full depth fillets. **b** Rounded adherend corners

Fig. 9 Enlarged section of a representative mesh for a single lap joint with full depth fillet. Additionally, a zoom focusing on the adhesive layer is provided



a draft of the investigated joint configuration are given in each diagram. Moreover, a representative figure of the predicted crack pattern for each of the studied joint end geometries is provided.

The first two experimental studies carried out by [da Silva et al. \(2006\)](#) and [Fernandes et al. \(2015\)](#) address the effects of the adhesive thickness and overlap length on the failure load of single lap joints with square ends without fillets, respectively. Steel as well as aluminum joints with the brittle adhesive AV138/HV998 are studied. Subsequently, the experimental test series by [Karachalios et al. \(2013\)](#) regarding the influence of the overlap length on the failure load of adhesive single lap joints with full depth fillets and high strength steel adherends is considered. Experimental results for the adhesives ESP110 and AV119 are taken into account for validation. In addition, the results addressing the effects of a full depth fillet on the failure load of adhesive single lap joints are investigated. Finally, the experimental campaign by [Zhao et al. \(2011b\)](#) addressing the influence of the adherend corners' rounding on the failure load and corresponding crack pattern is considered. They investigated single lap joints with aluminum adherends and the adhesive MY750. An overview on the investigated test series is given in [Table 1](#). Details of the respective experimental settings can be found in the associated references. The elastic properties and failure parameters of the considered adhesives are given

in [Table 2](#). For the adhesive MY750 the failure parameters are determined by a fit of the XFEM approach presented in [Sect. 3](#) to the experimental results of axially loaded single lap joints with square ends taken from the study by [Chen et al. \(2011\)](#). They studied two single lap joint configurations with steel and aluminum adherends with square ends and the adhesive MY750. Presuming $\mathcal{G}_{IIc} = 2\mathcal{G}_{Ic}$ which is a common simplifying assumption ([da Silva et al. 2006](#); [Campilho et al. 2009](#); [Lee et al. 2010](#)), the failure loads of the considered single lap joints are calculated using an enhanced XFEM approach ($F_{f,\text{pred}}^i$, $i = 1, 2$) for a wide range of $(\sigma_c, \mathcal{G}_{Ic})$ values. Here, the indices 1 and 2 denote the case of aluminum and steel adherends, respectively. Subsequently, the $(\sigma_c, \mathcal{G}_{Ic})$ couple which corresponds to the best prediction of the failure loads is determined minimizing the relative deviation between the predicted and the experimental failure loads:

$$\Delta_{\text{pred}} = \sqrt{\frac{1}{2} \sum_{i=1}^2 \left(\frac{F_{f,\text{pred}}^{(i)} - F_{f,\text{exp}}^{(i)}}{F_{f,\text{exp}}^{(i)}} \right)^2}. \quad (7)$$

The couple $(\sigma_c = 16 \text{ MPa}, \mathcal{G}_{Ic} = 0.4 \text{ N/mm})$ yields a deviation of $\Delta_{\text{pred},\text{min}} = 0.007$. The experimental deviation considering the experimental scatter gives

Table 1 Overview of investigated experimental test series

Reference	Adhesive	Fillet	Rounded corners	Parameter
da Silva et al. (2006)	AV138/HV998	w/o	w/o	t
Fernandes et al. (2015)	AV138/HV998	w/o	w/o	L
Karachalios et al. (2013)	ESP110	w/ and w/o	w/o	L
	AV119	w/	w/o	L
Zhao et al. (2011b)	MY750	w/	w/	r

Table 2 Material properties of the adhesives used in the experimental test series

Adhesive	E_a (GPa)	ν_a (-)	σ_c (MPa)	\mathcal{G}_{Ic} (N/mm)	\mathcal{G}_{IIc} (N/mm)	References
AV138/HV998	4.89	0.35	39.45	0.3	0.6	Campilho et al. (2011b) and da Silva et al. (2011)
AV119	3.45	0.37	67.1	1.07	3.85	da Silva et al. (2011) and Xu (2010)
ESP110	4.0	0.35	67	0.945	4.3	Hadavinia et al. (2006) and Blackman et al. (2005, 2008)
MY750	3.58	0.35	16 ^a	0.4 ^a	0.8 ^a	Chen et al. (2011)

^a Determined by an experimental fit to axially loaded single lap joints with square ends experimentally studied by Chen et al. (2011)

$$\Delta_{\text{exp}} = \sqrt{\frac{1}{2} \sum_{i=1}^2 \left(\frac{\Delta F_{f,\text{exp}}^{(i)}}{F_{f,\text{exp}}^{(i)}} \right)^2} = 0.0868 \quad (8)$$

providing an indication of the quality of the solution. The function Δ_{pred} with respect to the strength σ_c and toughness \mathcal{G}_{Ic} is shown in Fig. 10. Only the values for $\Delta_{\text{pred}} \leq \Delta_{\text{exp}}$ are shown for reasons of clarity. Note that the fitted fracture toughness value corresponds well to the toughness values found in literature, such as e.g. $\mathcal{G}_{Ic} = 0.38$ N/mm in the work by Chen et al. (2011) whereas the strength value for the cohesive segment is much lower than the data given in other works $\sigma_c \approx 84$ MPa (Harris and Adams 1985). The calculated failure parameters ($\sigma_c = 16$ MPa, $\mathcal{G}_{Ic} = 0.4$ N/mm) are considered for the subsequent failure load predictions of single lap joints with rounded adherend corners bonded with the adhesive MY750 in Sect. 4.3.

4.1 Adhesive single lap joints with square ends

At first, single lap joints with steel adherends and square ends are investigated. The steel adherends are modeled as linear elastic with Young’s modulus $E = 210$ GPa and Poisson’s ratio $\nu = 0.33$. The adhesive AV138/HV998 with the material parameters given in Table 2 is considered. Figure 11 shows the failure load predictions using the CZM as well as the

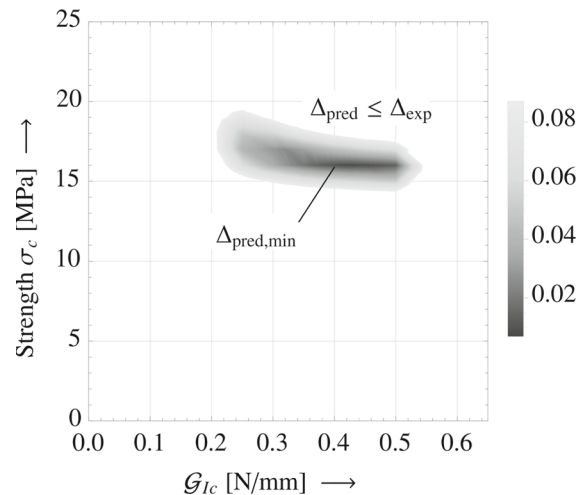


Fig. 10 Identification of the $(\sigma_c, \mathcal{G}_{Ic})$ values satisfying the condition $\Delta_{\text{pred}} \leq \Delta_{\text{exp}}$. The lowest value $\Delta_{\text{pred,min}}$ is found for the couple $(\sigma_c = 16$ MPa, $\mathcal{G}_{Ic} = 0.4$ N/mm)

enhanced XFEM approach in comparison with experimental results by da Silva et al. (2006). The numerical results of both approaches closely resemble each other and show a good agreement with the experimental results. The adhesive thickness effect is covered correctly: declining failure loads for increasing adhesive thicknesses are predicted. The predicted crack patterns of the CZM and the enhanced XFEM approach are very similar as well. The cracks emanate from both reentrant corners at which stress singularities are present,

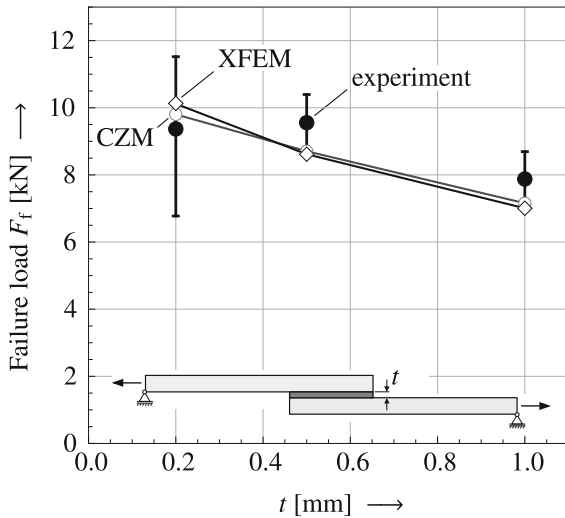


Fig. 11 Comparison between numerical strength predictions and experimental data from da Silva et al. (2006). The failure load is shown with respect to the adhesive thickness. Steel-AV 138-Steel single lap joint: $L = 25$ mm, $h_1 = h_2 = 2$ mm, $L_1 = L_2 = 95$ mm, $b = 25$ mm

cf. Fig. 12. Subsequently, the cracks propagate along the respective interfaces until they meet at the center of the overlap. The only difference in the crack patterns of both numerical approaches is found looking closer to the bi-material interface. In the case of the CZM approach with zero-thickness elements, the cracks propagate exactly along the bi-material interface whereas in the case of the enhanced XFEM approach the cracks propagate through the closest row of elements to the interface. However, providing a sufficiently fine mesh, both crack patterns almost coincide.

Figure 13 shows the results of a test series regarding the effect of the overlap length on the failure load of axially loaded single lap joints with square ends and AV138/HV998 as adhesive by Fernandes et al. (2015). Again, numerical results calculated with the CZM as well as the enhanced XFEM approach are compared to experimental data from literature. A very good agreement is obtained for both numerical approaches. The corresponding crack patterns show similar features as the ones of the Steel-AV138/HV998-Steel single lap joints shown above. The slight differences in the predicted failure loads of both numerical approaches are due to the different damage initiation criteria. The CZM approach uses a quadratic stress criterion whereas the XFEM approach considers damage onset if a maximum principal stress criterion is fulfilled. Implementing a quadratic stress criterion in the user subroutine

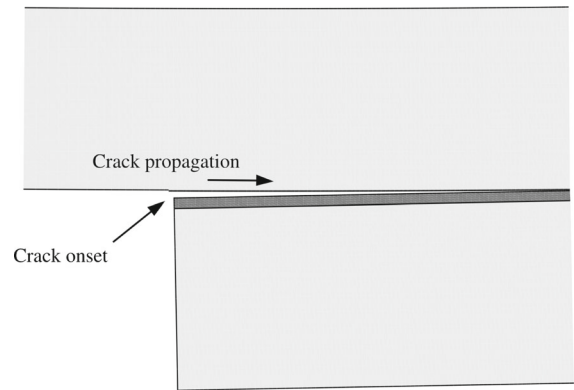


Fig. 12 Enlarged view of a typical crack pattern at the left end of an axially loaded single lap joint with square ends predicted by the enhanced XFEM approach. The arrows indicate the point of crack onset and subsequent crack propagation

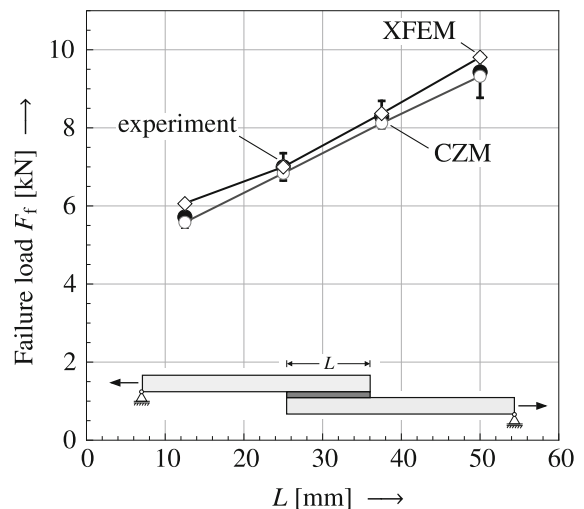


Fig. 13 Comparison between numerical strength predictions and experimental data given by Fernandes et al. (2015). The failure load is shown with respect to the overlap length. Aluminum-AV 138-Aluminum single lap joint: $h_1 = h_2 = 3$ mm, $t = 0.2$ mm, $L_1 + L + L_2 = 180$ mm, $b = 25$ mm

UDMGINI as a damage initiation criterion for the enhanced XFEM approach and providing a sufficiently fine mesh, the enhanced XFEM predicts the same failure loads as the CZM approach. However, predicting damage onset with a quadratic stress criterion with a crack direction perpendicular to the maximum principal stress does not seem to be consistent and is not based on a physical sound basis. Hence, the maximum principal stress criterion is used for the subsequent enhanced XFEM analyses.

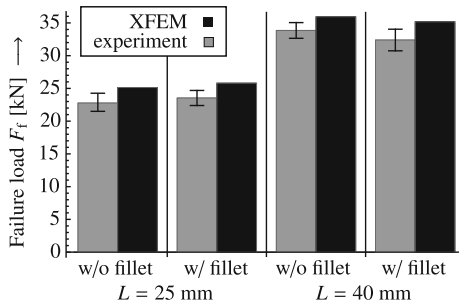


Fig. 14 Comparison between numerical strength predictions and experimental data from Karachalios et al. (2013). The failure loads are shown for single lap joints with and without fillets for two overlap lengths. Steel-ESP110-Steel single lap joints: $h_1 = h_2 = 1.6$ mm, $t = 0.1$ mm, $L_1 = L_2 = 63.5$ mm, $b = 25$ mm

4.2 Adhesive single lap joints with full depth fillets

The following studies show results for single lap joints with high strength steel adherends and full depth fillets, as depicted in Fig. 8a. The experimental campaign by Karachalios et al. (2013) is used for comparison with the numerical strength and crack pattern predictions by the enhanced XFEM approach. Karachalios et al. (2013) investigated the effects of a full depth fillet as well as the effects of the overlap length on

the failure load of axially loaded single lap joints. The present study considers two rather brittle adhesives ESP110 and AV119 in order to focus on crack onset and propagation and to avoid any pronounced non-linear effects. At first, a direct comparison of adhesive single lap joints with and without fillets is presented. Figure 14 shows the numerical strength predictions of single lap joints bonded with the adhesive ESP110 compared to experimental results by Karachalios et al. (2013). Obviously, the fillet has no major impact on the joint strength for the investigated configurations. Similar findings concerning the effects of full depth fillets in joints bonded with ESP110 were obtained by Grant et al. (2009) for mild steel adherends and small adhesive thicknesses. Grant et al. (2009) conclude that single lap joints with full depth fillets start to outperform joints with square ends only for sufficiently large adhesive thicknesses. However, the failure load predictions calculated with the enhanced XFEM approach are in a good agreement with the experimental results. The relative error between the predicted failure loads and the experimental mean values are less than 10%.

Figure 15a depicts the numerical and experimental results concerning the test campaign by Karachalios

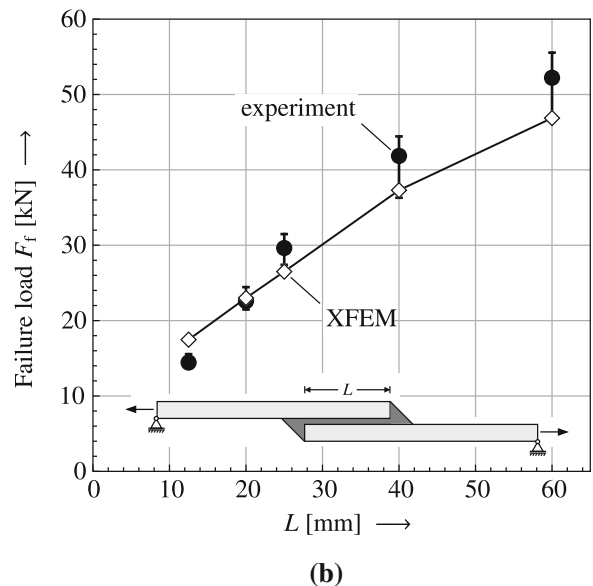
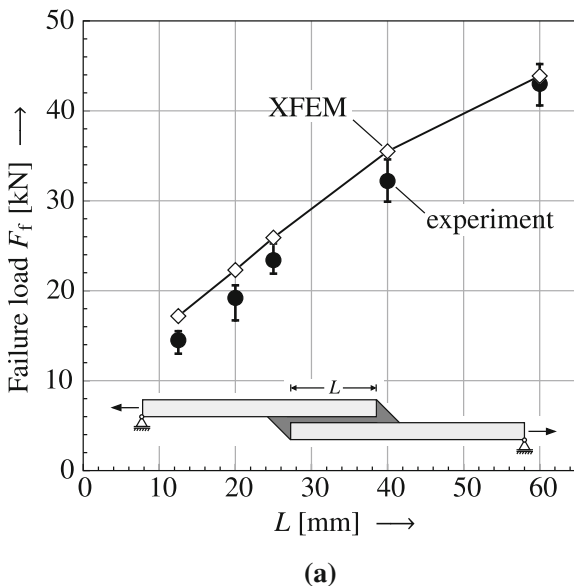


Fig. 15 Comparison between predictions and experimental data from Karachalios et al. (2013). The failure load is shown with respect to the overlap length. Steel-**a** ESP110/**b** AV119-Steel sin-

gle lap joint: $h_1 = h_2 = 1.6$ mm, $t = 0.1$ mm, $L_1 = L_2 = 63.5$ mm, $b = 25$ mm

and co-workers on the effects of the overlap length on the effective joint strength. Similar to the results shown in Fig. 14, the enhanced XFEM approach slightly overestimates the failure loads for joints bonded with ESP110, especially for short overlaps. However, the results are in a good to fair agreement to experimental data and the qualitative trend of increasing joint strengths with increasing overlap lengths are covered correctly. Similar findings are obtained for the joints bonded with the adhesive AV119. The crack patterns of all investigated single lap joints with full depth fillets show the same characteristic features. The final crack patterns are symmetric for all investigated adhesive joints. At the respective end of the overlap, a crack initiates at the embedded adherend corner within the adhesive layer as shown in Fig. 16. After crack onset, the joint could still support load indicating stable crack propagation within the adhesive. This corresponds well to the experimentally investigated phenomena of acoustic emission corresponding to crack initiation before final failure occurs (Karachalios et al. 2013; Zhao et al. 2011b). Subsequently, the crack propagates towards the free surface of the fillet in a 45° angle and towards the adherend-adhesive interface. Approaching the bi-material interface, the crack deflects and propagates along the adherend-adhesive interface. Reaching the outer surface of the fillet, a sudden rupture appears indicating that stable crack propagation has transitioned to unstable crack propagation and the joint finally fails. The predicted final crack pattern corresponds well to the findings by Adams and Harris (1987), Karachalios et al. (2013) and Mubashar et al. (2009, 2014).

4.3 Adhesive single lap joints with rounded adherend corners

In the following, more complex adherend geometries are investigated. Zhao et al. (2011b) experimentally studied the influence of the adherend corner curvature on the failure load of axially loaded single lap joints with fillets bonded with the adhesive MY750. Depending on the adherend corner curvature radius r , cf. Fig. 8b, different crack patterns occurred in the experiments. In the present study, single lap joints with the curvature radii $r = 0, 0.25, 1.6$ and 3.2 mm are investigated. Thereby, a curvature radius of 0 mm cor-

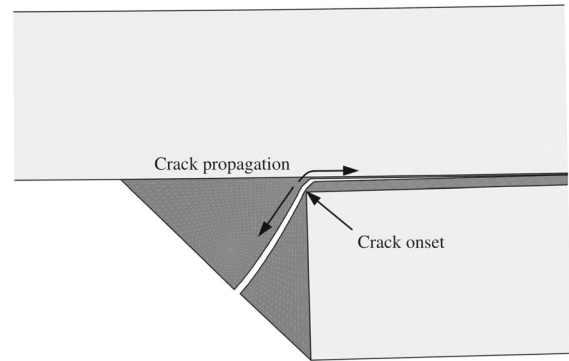


Fig. 16 Enlarged view of a typical crack pattern at the left end of an axially loaded single lap joint with full depth fillets. The arrows indicate the point of crack onset and subsequent crack propagation

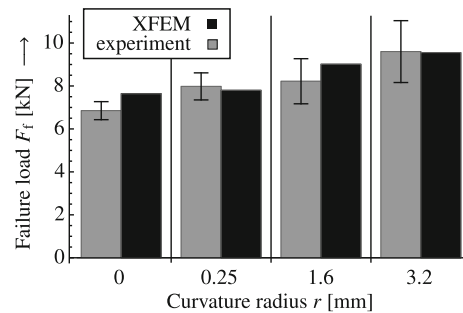


Fig. 17 Comparison between numerical strength predictions and experimental data from Zhao et al. (2011b). The failure loads are shown for single lap joints with fillets and different curvature radii of the adherend corners. Aluminum-MY750-Aluminum single lap joints: $h_1 = h_2 = 3.2$ mm, $t = 0.25$ mm, $L_1 = L_2 = 75$ mm, $b = 25$ mm

responds to sharp adherend corners. Figure 17 shows the numerical results for the investigated joint configurations compared to experimental data by Zhao et al. (2011b). A good agreement is achieved although the experimental fit of the failure parameters has been performed considering single lap joints without fillets and different adherend materials. The trend of increasing failure loads with increasing curvature radius has been captured correctly. For the single lap joint with square ends ($r = 0$ mm), the calculated crack pattern is similar to those of the other investigated joints with square ends and full depth fillets as depicted in Fig. 16. This finding corresponds well to the crack pattern observed in the corresponding experiments (Zhao et al. 2011b). The predicted crack path for the joint with small curvature radius $r = 0.25$ mm closely resembles those

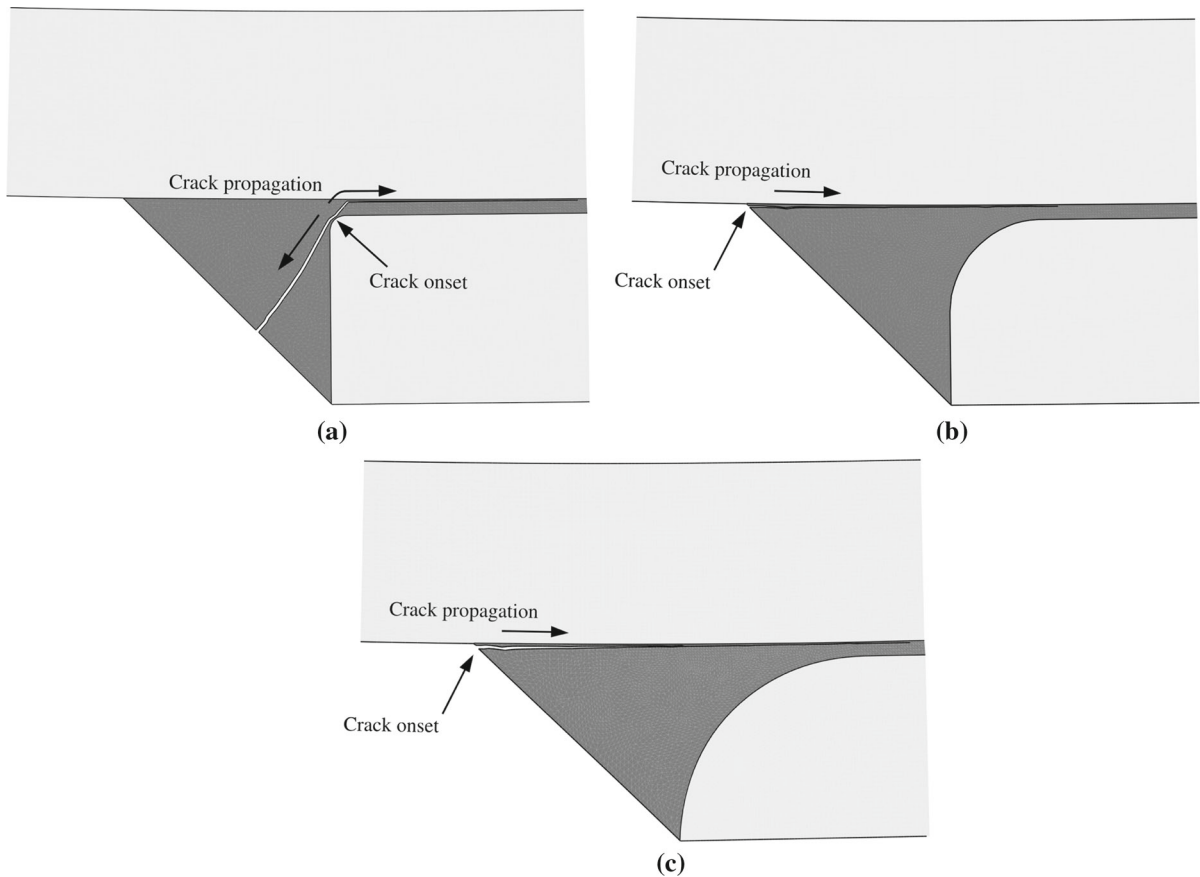


Fig. 18 Enlarged view of typical crack patterns at the left end of axially loaded single lap joints with full depth fillets and **a** small curvature radius ($r = 0.25$ mm), **b** medium curvature radius ($r = 1.6$ mm) and **c** large curvature radius ($r = 3.2$ mm) of the

adherend corner. The *arrows* indicate the point of crack onset and subsequent crack propagation. **a** Small radius. **b** Medium radius. **c** Large radius

for single lap joints with square ends, cf. Fig. 18a. Crack onset occurs in a 45° angle to the midplane of the joint and perpendicular to the adherend corners' rounding. Subsequently, the crack propagates towards the adherend-adhesive interface and the fillet free surface. Except for the vicinity of the locus of crack initiation, the crack is predicted to behave similar to the case of joints with square ends. Hence, a small rounding of the adherend corners has no major impact on the predicted crack pattern and yields only a slight increase in joint strength. Zhao et al. obtained quite similar results but observed that on one side of the joint the crack arrested meeting the adherend-adhesive interface whereas on the other side the crack was deflected and propagated along the adherend-adhesive interface until both cracks intersected. Possible explanations for

the unsymmetric failure pattern in spite of the symmetric configuration might be that both adherend surfaces show different properties such that crack arrest instead of deflection occurred, the adhesive is not cured under perfectly equal conditions resulting in an unhomogeneous distribution of residual stresses or the adherend corner's rounding is not equally generated. It is to note that it is quite difficult to obtain perfectly equal conditions concerning surface preparation and adhesive bonds in experiments. For the joint configuration with a medium adherend curvature radius $r = 1.6$ mm, a transition of the characteristic failure process is visible. The locus of crack onset is shifted from the rounded adherend corner to the edge of the fillet as shown in Fig. 18b. Due to the adherend rounding the stress concentration at the embedded adherend corner is reduced

to such an extent that the damage initiation criterion is first fulfilled at the edge of the fillet corresponding to the opposite adherend-adhesive interface. After crack onset, the crack propagates along the bi-material interface until the crack starting from the opposite end of the overlap is met. A similar crack pattern has been obtained for the single lap joint with maximum curvature radius $r = 3.2$ mm of the adherend corners, see Fig. 18c. This corresponds well to the observation by Zhao et al. (2011b) that there is no first crack apparent and that some of the cracks ran through the adhesive fillet along the adhesive-adherend interface. However, they also observed unsymmetric crack patterns with cracks emanating from the rounded adherend corner and propagating along the curved adherend to the edge of the fillet. Zhao et al. explained the occurrence of different crack patterns by air bubbles introduced during manufacture or residual thermal stresses in the fillets. However, the predicted crack path also corresponds well to the findings by Adams and Harris (1987) who predicted crack onset and propagation along the upper adherend-adhesive interface for aluminum/epoxy single lap joints with fillets and a large curvature radius.

5 Conclusion

In fracture processes of many joints or composite structures crack deflection plays an important role. To obtain realistic mechanism-based failure models computational analyses of such a crack growth are required. The eXtended finite element method (XFEM) is widely used to study crack growth but currently available implementations cannot render the effect of crack deflection at interfaces. In adhesive joint design studies, it has been shown that XFEM analyses predict cracks that approach the interfaces and no further crack advance can be predicted. The present enhanced XFEM framework uses an Abaqus user subroutine to alter the crack growth prediction along interfaces such that cracks are deflected at interfaces but are also able to leave the interface at a later point. The given approach is restricted to multi-material configurations in which it is known that cracks only occur in certain materials. Such an assumption is legitimate in many engineering cases as e.g. joints with metallic adherends and polymer adhesives or fibre reinforced plastic composites. The framework is generally applicable to any crack growth analyses and does not require more user input

than a classical XFEM analysis. The present framework is described for the case of two-dimensional crack initiation and growth problems but can easily be extended to the full 3D case. The given approach has been validated by comparison to experimental results. Focussing on adhesive lap joints several different experimental campaigns were analysed. The almost plane crack growth observed in the experiments could be reproduced very well by the given two dimensional computational failure model. The obtained crack paths and the corresponding failure loads show good agreements to experimental results.

The given model enables studying the complex failure processes in adhesive joints and allows for parameter studies for joint improvement or design studies. It could also be used in automated optimization routines that would allow for identifying joint designs that are most adapted to the considered loading case. The framework can also be applied for the study of micro-mechanical failure processes that occur in multi-material structures. Among these are structures that are made of several constituents to improve the functional properties or that contain unwanted contaminations as e.g. hard inclusions.

References

- Adams RD, Peppiatt N (1974) Stress analysis of adhesive-bonded lap joints. *J Strain Anal Eng Des* 9(3):185–196
- Adams RD, Harris JA (1987) The influence of local geometry on the strength of adhesive joints. *Int J Adhes Adhes* 7(2):69–80
- Adams RD, Atkins RW, Harris JA, Kinloch AJ (1986) Stress analysis and failure properties of carbon-fibre-reinforced-plastic/steel double-lap joints. *J Adhes* 20(1):29–53
- Belytschko T, Black T (1999) Elastic crack growth in finite elements with minimal remeshing. *Int J Numer Methods Eng* 45(5):601–620
- Blackman BRK, Kinloch AJ, Paraschi M (2005) The determination of the mode II adhesive fracture resistance, G_{IIc} , of structural adhesive joints: an effective crack length approach. *Eng Fract Mech* 72(6):877–897
- Blackman BRK, Johnsen BB, Kinloch AJ, Teo WS (2008) The effects of pre-bond moisture on the fracture behaviour of adhesively-bonded composite joints. *J Adhes* 84(3):256–276
- Bigwood DA, Crocombe AD (1990) Non-linear adhesive bonded joint design analyses. *Int J Adhes Adhes* 10(1):31–41
- Bush MB (1997) The interaction between a crack and a particle cluster. *Int J Fract* 88:215–232
- Campilho RDSG, de Moura MFSF, Domingues JJMS (2009) Numerical prediction on the tensile residual strength of

- repaired CFRP under different geometric changes. *Int J Adhes Adhes* 29(2):195–205
- Campilho RDSG, Banea MD, Chaves FJP, da Silva LFM (2011a) Extended finite element method for fracture characterization of adhesive joints in pure mode I. *Comput Mater Sci* 50(4):1543–1549
- Campilho RDSG, Banea MD, Pinto AMG, da Silva LFM, de Jesus AMP (2011b) Strength prediction of single- and double-lap joints by standard and extended finite element modeling. *Int J Adhes Adhes* 31(5):363–372
- Campilho RDSG, Banea MD, Neto JABP, da Silva LFM (2013a) Modelling adhesive joints with cohesive zone models: effect of the cohesive law shape of the adhesive layer. *Int J Adhes Adhes* 44:48–56
- Campilho RDSG, Banea MD, da Silva LFM (2013b) Tensile behaviour of a structural adhesive at high temperatures by the extended finite element method. *J Adhes* 89(7):529–547
- Chawla BN, Shen YL (2001) Mechanical behavior of particle reinforced metal matrix composites. *Adv Eng Mater* 3(6):357–370
- Chen Z, Adams RD, da Silva LFM (2011) Fracture toughness of bulk adhesives in mode I and mode III and curing effect. *Int J Fract* 167(2):221–234
- Crocombe AD, Adams RD (1981) Influence of the spew fillet and other parameters on the stress distribution in the single lap joint. *J Adhes* 13(2):141–155
- da Silva LFM, Adams RD (2007) Techniques to reduce the peel stresses in adhesive joints with composites. *Int J Adhes Adhes* 27(3):227–235
- da Silva LFM, Rodrigues TNSS, Figueiredo MAV, de Moura MFSF, Choual JAG (2006) Effect of adhesive type and thickness on the lap shear strength. *J Adhes* 82:1091–1115
- da Silva LFM, Campilho RDSG (2012) Advances in numerical modeling of adhesive joints. Springer, Heidelberg
- da Silva LFM, das Neves PJC, Adams RD, Wang A, Spelt JK (2009) Analytical models of adhesively bonded joints—part II: comparative study. *Int J Adhes Adhes* 29(3):331–341
- da Silva LFM, Öchsner A, Adams RD (2011) Handbook of adhesion technology. Springer, Heidelberg
- Fernandes TAB, Campilho RDSG, Banea MD, da Silva LFM (2015) Adhesive selection for single lap bonded joints: experimentation and advanced techniques for strength prediction. *J Adhes* 91(10–11):841–862
- Fernlund G, Spelt JK (1991) Failure load prediction of structural adhesive joints: part 1: analytical method. *Int J Adhes Adhes* 11(4):213–220
- Goglio L, Rossetto M, Dragoni E (2008) Design of adhesive joints based on peak elastic stresses. *Int J Adhes Adhes* 28(8):427–435
- Gonçalves JPM, de Moura MFSF, de Castro PMST, Marques AT (2000) Interface element including point to surface constraints for three dimensional problems with damage propagation. *Eng Comput* 17(1):28–47
- Grant LDR, Adams RD, da Silva LFM (2009) Effect of the temperature on the strength of adhesively bonded single lap and T joints for the automotive industry. *Int J Adhes Adhes* 29(5):535–542
- Hadavinia H, Kawashita L, Kinloch AJ, Moore DR, Williams JG (2006) A numerical analysis of the elastic–plastic peel test. *Eng Fract Mech* 73(16):2324–2335
- Harris JA, Adams RD (1984) Strength prediction of bonded single lap joints by non-linear finite element methods. *Int J Adhes Adhes* 4(2):65–78
- Harris JA, Adams RD (1985) An assessment of the impact performance of bonded joints for use in high energy absorbing structures. *Proc Inst Mech Eng Part C J Mech Eng Sci* 199(2):121–131
- Hell S, Weißgraeber P, Felger J, Becker W (2014) A coupled stress and energy criterion for the assessment of crack initiation in single lap joints: a numerical approach. *Eng Fract Mech* 117:112–126
- Hildebrand M (1994) Non-linear analysis and optimization of adhesively bonded single lap joints between fibre-reinforced plastics and metals. *Int J Adhes Adhes* 14(4):261–267
- Lee MJ, Cho TM, Kim WS, Lee BC, Lee JJ (2010) Determination of cohesive parameters for a mixed-mode cohesive zone model. *Int J Adhes Adhes* 30(5):322–328
- Karachalios EF, Adams RD, da Silva LFM (2013) Single lap joints loaded in tension with high strength steel adherends. *Int J Adhes Adhes* 43:81–95
- Kitey R, Phan AV, Tippur HV, Kaplan T (2006) Modeling of crack growth through particulate clusters in brittle matrix by symmetric-Galerkin boundary element method. *Int J Fract* 141(1–2):11–25
- Leguillon D (2002) Strength or toughness? A criterion for crack onset at a notch. *Eur J Mech A Solids* 21(1):61–72
- Liljedahl CDM, Crocombe AD, Wahab MA, Ashcroft IA (2006) Damage modeling of adhesively bonded joints. *Int J Fract* 141(1–2):147–161
- Melenk J, Babuška I (1996) The partition of unity finite element method: basic theory and applications. *Comput Methods Appl Mech Eng* 139(1):289–314
- Moës N, Dolbow J, Belytschko T (1999) A finite element method for crack growth without remeshing. *Int J Numer Methods Eng* 46(1):131–150
- Moradi A, Carrère N, Leguillon D, Martin E, Cognard JY (2013) Strength prediction of bonded assemblies using a coupled criterion under elastic assumptions: effect of material and geometrical parameters. *Int J Adhes Adhes* 47:73–82
- Mubashar A, Ashcroft IA, Critchlow GW, Crocombe AD (2009) Modelling moisture absorption–desorption effects in adhesive joints. *Int J Adhes Adhes* 29(8):751–760
- Mubashar A, Ashcroft IA, Crocombe AD (2014) Modelling damage and failure in adhesive joints using a combined XFEM-cohesive element methodology. *J Adhes* 90:682–697
- Osher S, Sethian JA (1998) Fronts propagating with curvature-dependent speed: algorithms based on Hamilton–Jacobi formulations. *J Comput Phys* 79(1):12–49
- Remmers JJC, de Borst R, Needleman A (2008) The simulation of dynamic crack propagation using the cohesive segments method. *J Mech Phys Solids* 56(1):70–92
- Shahin K, Taheri F (2008) The strain energy release rates in adhesively bonded balanced and unbalanced specimens and lap joints. *Int J Solids Struct* 45(25):6284–6300
- Song JH, Areias PMA, Belytschko T (2006) A method for dynamic crack and shear band propagation with phantom nodes. *Int J Numer Methods Eng* 67(6):868–893
- Stein N, Weißgraeber P, Becker W (2015) A model for brittle failure in adhesive lap joints of arbitrary joint configuration. *Compos Struct* 133:707–718

- Stein N, Weißgraeber P, Becker W (2016) Brittle failure in adhesive lap joints—a general finite fracture mechanics approach. *Proced Struct Integr* 2:1967–1974
- Stuparu FA, Apostol DA, Constantinescu DM, Picu CR, Sandu M, Soroohan S (2016a) Cohesive and XFEM evaluation of adhesive failure for dissimilar single-lap joints. *Proced Struct Integr* 2:316–325
- Stuparu FA, Constantinescu DM, Apostol DA, Sandu M (2016b) A combined cohesive elements—XFEM approach for analyzing crack propagation in bonded joints. *J Adhes* 92(7–9):535–552
- Sukumar N, Prévost JH (2003) Modeling quasi-static crack growth with the extended finite element method. Part I: computer implementation. *Int J Solids Struct* 40(26):7513–7537
- Sukumar N, Huang ZY, Prévost JH, Suo Z (2004) Partition of unity enrichment for bimaterial interface cracks. *Int J Numer Methods Eng* 59(8):1075–1102
- Tsai M, Morton J (1995) The effect of a spew fillet on adhesive stress distributions in laminated composite single-lap joints. *Compos Struct* 32(1–4):123–131
- Turon A, Dávila CG, Camanho PP, Costa J (2007) An engineering solution for mesh size effects in the simulation of delamination using cohesive zone models. *Eng Fract Mech* 74(10):1665–1682
- Wang Z, Ma L, Wu L, Yu H (2012) Numerical simulation of crack growth in brittle matrix of particle reinforced composites using the XFEM technique. *Acta Mech Solida Sin* 25(1):9–21
- Weißgraeber P, Leguillon D, Becker W (2016) A review of finite fracture mechanics: crack initiation at singular and non-singular stress raisers. *Arch Appl Mech* 86(1–2):375–401
- Xu B (2010) Fracture mechanisms and failure criteria of adhesive joints and toughened epoxy adhesives. Dissertation, Queen Mary College, London
- Zhao X, Adams RD, da Silva LFM (2011a) Single lap joints with rounded adherend corners: stress and strain analysis. *J Adhes Sci Technol* 25(8):819–836
- Zhao X, Adams RD, da Silva LFM (2011b) Single lap joints with rounded adherend corners: experimental results and strength prediction. *J Adhes Sci Technol* 25(8):837–856